ADVANCES IN ATMOSPHERIC SCIENCES, VOL. 32, AUGUST 2015, 1129–1142

Simulation of the Equatorially Asymmetric Mode of the Hadley Circulation in CMIP5 Models

FENG Juan[1,2,3], LI Jianping*[1,3], ZHU Jianlei[2], LI Fei[4], and SUN Cheng[1,3]

[1]*College of Global Change and Earth System Science, Beijing Normal University, Beijing* 100875
[2]*State Key Laboratory of Numerical Modeling for Atmospheric Sciences and Geophysical Fluid Dynamics, Institute of Atmospheric Physics, Chinese Academy of Sciences, Beijing* 100029
[3]*Joint Center for Global Change Studies, Beijing* 100875
[4]*Department of Lower Atmosphere Observation Research, Institute of Atmospheric Physics, Chinese Academy of Sciences, Beijing* 100029

(Received 14 July 2014; revised 26 December 2014; accepted 5 January 2015)

ABSTRACT

The tropical Hadley circulation (HC) plays an important role in influencing the climate in the tropics and extra-tropics. The realism of the climatological characteristics, spatial structure, and temporal evolution of the long-term variation of the principal mode of the annual mean HC (i.e., the equatorially asymmetric mode, EAM) was examined in model simulations from the Coupled Model Intercomparison Project Phase 5 (CMIP5). The results showed that all the models are moderately successful in capturing the HC's climatological features, including the spatial pattern, meridional extent, and intensity, but not the spatial or temporal variation of the EAM. The possible reasons for the poor simulation of the long-term variability of the EAM were explored. None of the models can successfully capture the differences in the warming rate between the tropical Southern Hemisphere (SH) and Northern Hemisphere (NH), which is considered to be an important driver for the variation of the AM. Most of the models produce a faster warming in the NH than in the SH, which is the reverse of the observed trend. This leads to a reversed trend in the meridional gradient between the SH and NH, and contributes to the poor simulation of EAM variability. Thus, this aspect of the models should be improved to provide better simulations of the variability of the HC. This study suggests a possible reason for the poor simulation of the HC, which may be helpful for improving the skill of the CMIP5 models in the future.

Key words: tropical Hadley circulation, equatorially asymmetric mode, CMIP5, sea surface temperature

Citation: Feng, J., J. P. Li, J. L. Zhu, F. Li, and C. Sun, 2015: Simulation of the equatorially asymmetric mode of the Hadley circulation in CMIP5 models. *Adv. Atmos. Sci.*, **32**(8), 1129–1142, doi: 10.1007/s00376-015-4157-0.

1. Introduction

The Hadley circulation (HC) is the largest atmospheric circulation system on the planet, and is defined as the zonal-mean meridional mass circulation in the atmosphere bounded approximately by 30°S and 30°N. The HC is a thermally driven meridional circulation with poleward mass transport in the upper troposphere and equatorward mass transport in the lower troposphere (Quan et al., 2004). The HC plays an essential role in influencing the climate at low, mid, and high latitudes, and is thus of great importance to the global climate (e.g., Lindzen, 1994; Chang, 1995; Hou, 1998; Diaz and Bradley, 2004; Feng et al., 2013).

Recently, the long-term variability of the HC has been studied intensively, with the width and intensity of the HC being the key issues (Hu and Zhou, 2009). Many studies, using a variety of observational and reanalysis data, have consistently shown that the width of the HC shows an obvious poleward expansion trend, and the rate of expansion has been quantified (Fu et al., 2006; Hudson et al., 2006; Frierson et al., 2007; Lu et al., 2007; Seidel et al., 2008; Johanson and Fu, 2009; Hu et al., 2011). In terms of intensity, observations show enhanced average annual HC intensity in the 1990s (Chen et al., 2002; Wielicki et al., 2002). The significant increasing trend of the Northern Hemisphere (NH) winter HC can be traced back to the 1950s (Quan et al., 2004; Ma and Li, 2008; Hu and Zhou, 2009). However, the intensity of the boreal summer HC shows no obvious trend (Quan et al., 2004; Feng et al., 2011). Furthermore, the intensity of the HC since 1979 has been examined (Stachnik and Schumacher, 2011; Nguyen et al., 2013), revealing inconsistent trends among different datasets.

In addition to its intensity and width, the spatial struc-

* Corresponding author: LI Jianping
Email: ljp@bnu.edu.cn

ture of the long-term variability is another important aspect of the HC, and has received considerable attention in recent years. The annual cycle of the HC consists of equatorially symmetric and asymmetric parts (Dima and Wallace, 2003). More recently, the first principal mode of the long-term variability of the HC was found to be equatorially asymmetric in both boreal winter and summer, with variability that is considered to be closely related to the sea surface temperature (SST) over the Indo-Pacific warm pool (IPWP; Ma and Li, 2008; Feng et al., 2011). A further study by Li and Feng (2015) indicated that the faster warming of SST within the IPWP in the Southern Hemisphere (SH), as compared to the NH, is responsible for the variation of the equatorially asymmetric mode (EAM) in both boreal winter and summer. Feng et al. (2013) also studied the long-term variability of the boreal spring HC, and reported that the structure of the principal mode of the HC is also equatorially asymmetric. They found that the long-term strengthening trend in the AM contributes to frequent droughts in the extra-tropics during boreal spring. These studies raise the possibility that the spatial structure of the principal mode of the HC is independent of its climatological structure, and that the unequal warming in the tropical NH and SH may contribute to its long-term variability. This possibility is further supported by the findings of Feng and Li (2013), who investigated the influence of different types of El Niño–Southern Oscillation events on the HC, and revealed that the spatial structure of the SST meridional gradient is responsible for the spatial anomalies of the HC.

The above review of the present status of HC research suggests that the variability of the HC is complex. Given that the variation of the HC is closely linked to changes in global atmospheric circulation, and has major impacts on weather and climate on the global scale, it is important to understand the long-term variability of the HC as well as its future changes. Of more practical importance, if numerical models can successfully simulate the variation of the HC, this would be of great interest for identifying and understanding the changes in the HC, and would also be important for predicting future climate change. Recent work by Hu et al. (2013) discussed Coupled Model Intercomparison Project Phase 5 (CMIP5) simulations of the poleward expansion of the HC, and reported that the simulated poleward expansion in CMIP5 is much weaker than in observations. However, few studies evaluating model performance have focused on the spatial structure of the principal mode of long-term HC variability. Such an approach would not only improve understanding of the variability of the HC, but would also provide some reference points for improvements to climate models.

CMIP5 has provided a comprehensive evaluation of state-of-the-art multi-model datasets of coupled general circulation models (CGCMs), and has proved to be a useful benchmark for model sensitivity and predictability experiments to SST forcing (Taylor et al., 2012). However, current climate models still possess clear deficiencies in simulating the variability of climatic modes (Guo et al., 2013; Zheng et al., 2013; Zhu et al., 2013). Although considerable advances have been made in improving the performance of CGCMs, relatively little effort has been directed toward obtaining a proper simulation of the long-term variation of climatic circulation. In the present study, the performance of CGCMs in simulating the complex long-term variation of the HC, in particular the primary mode of the annual mean HC, is examined with the aim of identifying the possible causes of unsatisfactory simulations, and thus contribute to the improvement of current CGCMs.

The remainder of the paper is organized as follows. Section 2 describes the models, observational datasets, and methods used in the study. Section 3 outlines the performance of CMIP5 models in reproducing the spatial and temporal evolution of the EAM of the HC. Section 4 discusses the possible causes of unsatisfactory simulation of the EAM. And finally, conclusions and further discussion are provided in section 5.

2. Models, observational datasets, and methodology

2.1. *Models*

CMIP5 has brought together more than 20 international climate modeling centers to conduct a comprehensive set of long-term simulations of 20th century climate and different climate change scenarios in the 21st century. CMIP5 is a standard experimental protocol for global CGCMs. It provides a community-based infrastructure in support of climate model diagnosis, intercomparison, validation, data access, and documentation.

The simulations from 10 coupled models developed at different modeling centers (see Table 1) were used in the present study. Models were selected on the basis of data availability and model diversity. Considering that the simulation periods for each model are different, the model simulations of monthly meridional wind and surface temperature from January 1961 to December 2000 were chosen to provide a common study period. Multiple simulations are available from most models, with different realizations based on different initial conditions, but only the first standard simulations were used in this study.

2.2. *Observational datasets*

The reanalysis data used in this study were from the National Centers for Environmental Prediction/National Center for Atmospheric Research (NCEP/NCAR) dataset, from the late 1940s to the present day (Kalnay et al., 1996). The 40-year European Centre for Medium-Range Weather Forecasts Reanalysis (ERA40) from 1958 to mid-2002 (Uppala et al., 2005) was also used to verify the long-term variation of the HC. Two SST datasets were extracted: one from the Met Office Hadley Centre Sea Ice and SST dataset version 1, on a $1^\circ \times 1^\circ$ latitude–longitude grid (HadISST; Rayner et al., 2003), and the other from the Improved Extended Reconstruction SST dataset (ERSST; Smith and Reynolds, 2004) with $2^\circ \times 2^\circ$ horizontal resolution, to explore and confirm the impacts of tropical SST on the long-term variability of the HC. Based on the coverage and availability of the model

Table 1. List of the CMIP5 models used in this study.

Name	Abbreviation	Source	Horizontal resolution (lon×lat)	Vertical Levels	Reference
Beijing Climate Center, Climate System Model	BCC-CSM1-1	Beijing Climate Center, China	128 × 64	17	Jiang et al. (2010)
Beijing Climate Center, Climate System Model	BCC-CSM1-1-m	Beijing Climate Center, China	320 × 160	17	Jiang et al. (2010)
Fourth Generation Canadian Coupled Model	CANCM4	Canadian Centre for Climate Modelling and Analysis, Canada	128 × 64	22	Chylek et al. (2011)
Second Generation Canadian Earth System Model	CANESM2	Canadian Centre for Climate Modelling and Analysis, Canada	128 × 64	22	Chylek et al. (2011)
Center National de Recherches Météorologiques Coupled Global Climate Model	CNRM-CM5	Centre National de Recherches Météorologiques, France	256 × 128	17	Voldoire et al. (2013)
The First Institution of Oceanography Earth System Model	FIO-ESM	The First Institution of Oceanography, China	128 × 64	17	Qiao et al. (2013)
Flexible Global Ocean-Atmosphere-Land System Model	FGOALS-s2	Institute of Atmospheric Physics, Chinese Academy of Sciences, China	128 × 108	17	Bao et al. (2013)
Institute for Numerical Mathematics Coupled Model	INMCM4	Institute for Numerical Mathematics, Russia	180 × 120	17	Volodin et al. (2010)
Max Planck Institute Earth System Model	MPI-ESM-MR	Max Planck Institute for Meteorology	192 × 96	25	Stevens et al. (2013)
Norwegian Climate Centre Earth System Model	NORESM1-M	Norwegian Climate Centre	144 × 96	17	Bentsen et al. (2012)

simulations and reanalysis data, the period 1961–2000 was selected to examine the long-term variability of the principal mode of the annual mean HC, and to evaluate the simulation performance of the CMIP5 models.

2.3. *Methodology*

The HC was characterized by the mass stream function (MSF) of the mean meridional circulation (MMC). The MSF was obtained by vertically integrating the zonal-mean meridional winds in the conventional way (Li, 2001), and was defined by

$$\psi = \int \frac{2\pi R\cos\phi}{g}[\overline{v}]dp, \qquad (1)$$

where R is the mean radius of the earth, ϕ is the latitude, $[\overline{v}]$ is the zonal mean meridional wind, g is the gravitational acceleration, and p the pressure. The operators $\overline{\ }$ and [ ] represent temporal and zonal averaging, respectively. As the annual mean HC has a two-cell structure and tends to be symmetric about the equator (Figs. 1 and 2), and to avoid one cell dominating the calculated intensity, the HC intensity (HCI) was calculated separately in the NH and SH, and defined as the maximum of the absolute value of the annual mean MSF in each hemisphere. The locations of the poleward edges and ascending branch of the HC were identified as the latitudes where the MSF reached zero at 500 hPa. These were obtained using linear interpolation, and then the width of the HC could be derived from the differences between the poleward edge locations in each hemisphere.

EOF analysis was employed to determine the principal mode of year-to-year variability of the annual mean MMC. North's rule was employed to determine whether the EOF modes could be significantly separated. That is, the adjacent significant separated modes of the EOF's eigenvalues should satisfy the relation

$$\Delta\lambda_j = \lambda_j\sqrt{\frac{2}{N}}\ , \quad \lambda_{j+1} - \lambda_j \geqslant \Delta\lambda_j\ ,$$

where λ is the eigenvalue, and N is the valid degrees of freedom. The relationship between the principal mode of the annual mean HC and SST was investigated by correlation analysis. Linear trends were computed using least-squares linear regression. The statistical significance of the values of the correlations and linear trends was assessed by means of the two-sided Student's t-test.

3. Performance of CMIP5 models in reproducing the EAM of the annual mean HC

3.1. *Climatological HC simulated by CMIP5 models*

The southern component of the HC based on ERA40 data is more intense than that based on NCEP/NCAR data, but nonetheless there is good agreement between the spatial patterns of the HC (Figs. 1a and b). The northern and southern components of the HC have equivalent extent and magnitude, with descending branches around 30° latitude in each hemisphere and an ascending branch near the equator.

Similar characteristics are seen in the climatological mean for all the models, with equivalent magnitudes of the northern and southern components of the HC and similar meridional extents (Fig. 2). However, there are small differences in the actual values of the HC extent. The narrowest HC extent is found in FIO-ESM, while the widest is

Table 2. Locations of the southern and northern edges and the ascending branch of the climatological Hadley circulation (HC), together with its extent and intensity (HCI). The HCIs of both the Southern Hemisphere (SH) and Northern Hemisphere (NH) are shown. The numbers in parentheses are the corresponding standard deviations; R1 is the correlation of the PCs of the long-term variability of the annual mean HC between observations and models; R2 is the spatial correlation of SST trends between observations and models within the range (20°S–20°N, 0°–358°E).

Source	Southern edge	Ascending edge	Northern edge	Extent	HCI (SH)	HCI (NH)	R1	R2
NCEP/NCAR	31.32°S (0.69°)	5.69°N (1.35°)	29.82°N (0.54°)	61.14° (1.07°)	8.55 (0.54)	6.91 (0.58)		
ERA40	30.73°S (0.66°)	5.80°N (1.39°)	29.92°N (1.07°)	62.13° (1.36°)	11.57 (1.03)	8.70 (1.01)		
BCC-CSM1-1	30.02°S	2.83°N	29.22°N	59.24°	9.33	8.72	0.12	0.68
BCC-CSM1-1-m	32.14°S	3.87°S	30.99°N	63.13°	9.25	10.06	−0.07	0.54
CANCM4	31.20°S	4.86°N	28.55°N	59.75°	11.40	9.44	0.03	0.36
CANESM2	31.31°S	4.03°N	28.89°N	60.20°	11.52	9.36	−0.09	0.34
CNRM-CM5	29.70°S	3.51°N	27.83°N	57.53°	10.46	9.89	−0.05	0.41
FIO-ESM	29.51°S	2.46°N	27.19°N	56.70°	12.74	10.36	0.02	0.46
FGOALS-s2	29.46°S	7.10°N	28.43°N	57.89°	10.66	7.81	−0.34	0.55
INMCM4	32.18°S	1.98°S	28.53°N	60.71°	7.60	7.40	−0.13	0.44
MPI-ESM-MR	30.47°S	7.25°N	29.41°N	59.88°	10.64	8.23	−0.08	0.63
NORESM1-M	32.19°S	0.40°S	30.34°N	62.53°	11.19	10.68	0.16	0.37

in BCC-CSM1-1-m (Table 2). However, the differences between the results based on observations and models lie mostly within two standard deviations, except for CNRM_CM5 and FIO_ESM, implying that the model simulations of the climatological structure of the HC are reliable. Note that there are large differences between the observations for the climatological HCI: the values of HCI based on ERA40 are much larger than those based on NCEP/NCAR in both hemispheres—a discrepancy reported previously in Feng et al. (2011) for boreal summer. However, both reanalyses show that the intensity of the southern cell is stronger than the northern cell. Most of the HCI model values are within the range of NCEP/NCAR and ERA40, except for those of FIO-ESM and INMCM4. The stronger southern cell is captured in all

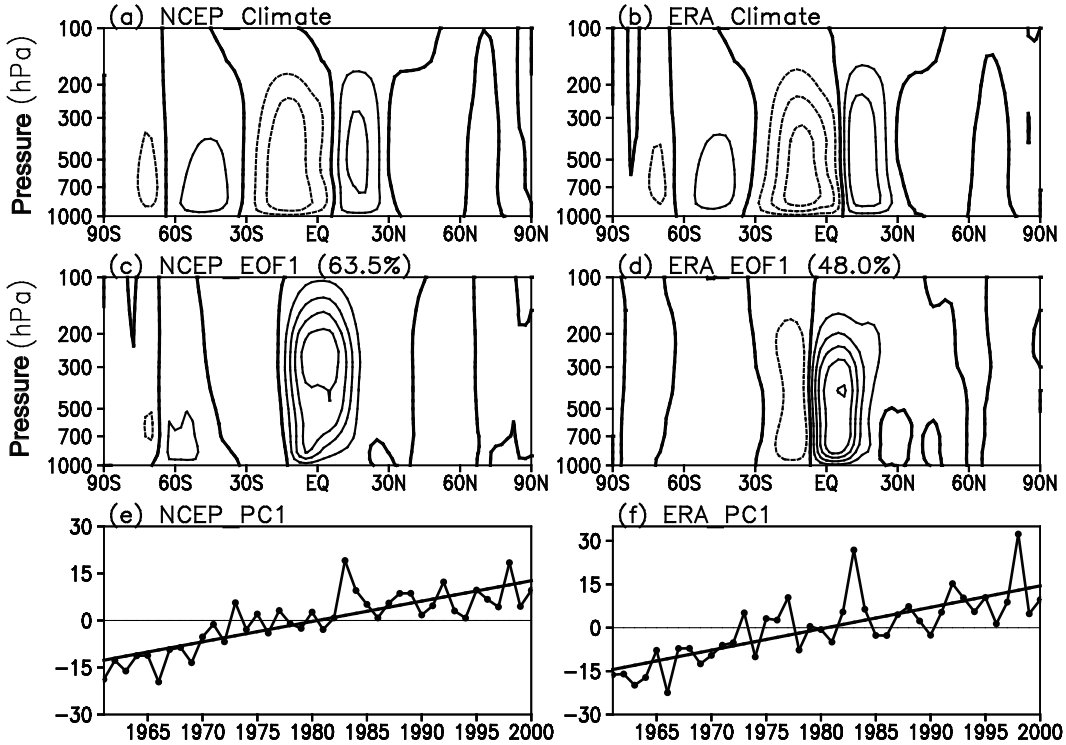

Fig. 1. (a) The climatological mean of the annual mean mass stream function (MSF) determined from NCEP/NCAR data. The contour interval is 3×10^{10} kg s^{-1}, and the solid (dotted) contours indicate positive (negative) values. (c) As in (a), but for the first principal mode of the annual mean MSF and the explained variance (%). The contour interval is 0.03×10^{10} kg s^{-1}. (e) Time series of the principal mode of the annual mean. The solid line is the linear trend, significant at the 0.05 level. (b, d, f) As in (a, c, e), but based on ERA40 data.

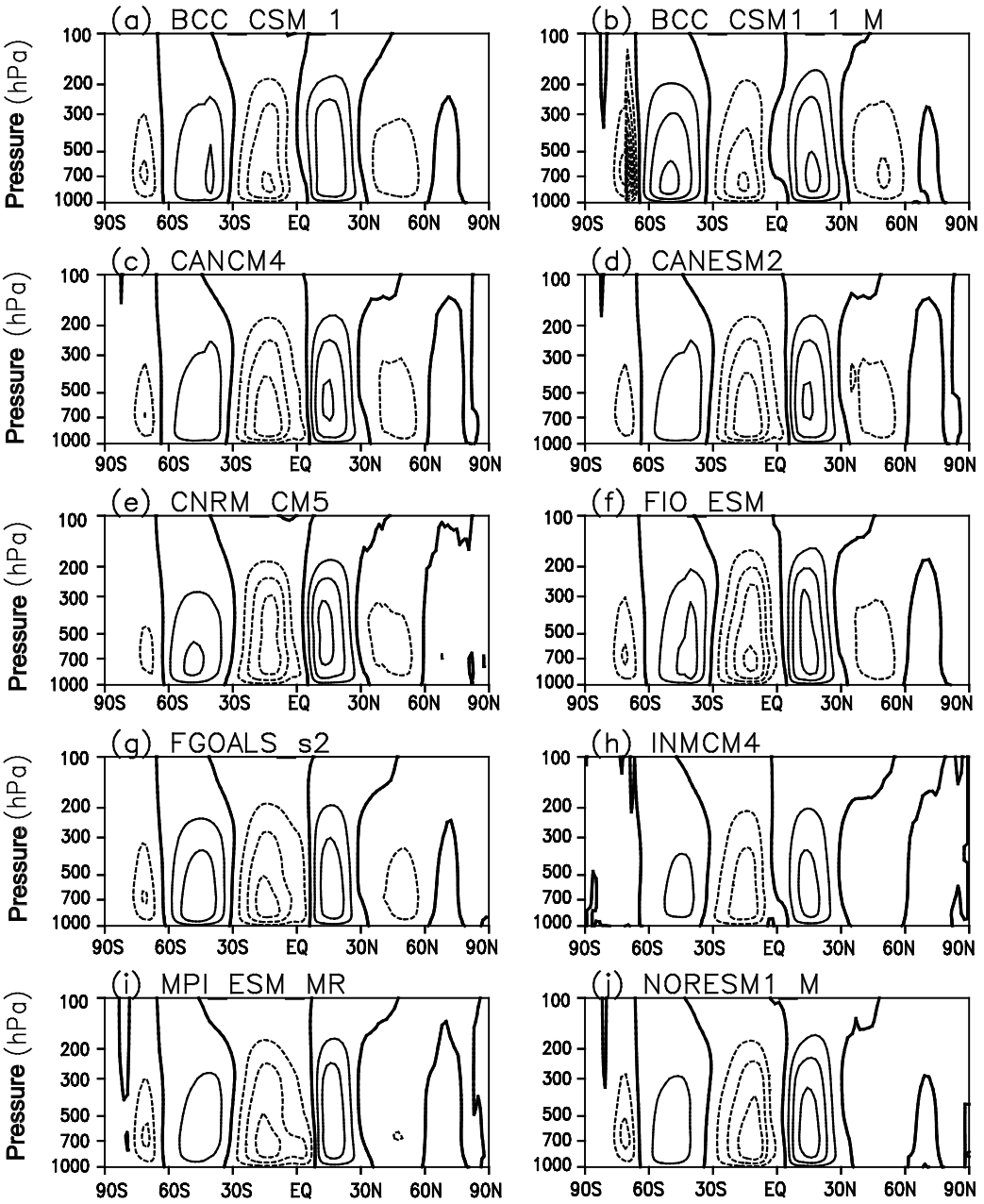

Fig. 2. As in Fig. 1a, but for the climatological mean of the annual mean MSF determined from CMIP5 models over the period 1961–2000.

models, and the differences among models in this regard are negligible. This result indicates that the models possess moderate capability in depicting the climatological structures of the HC.

3.2. *Evaluation of the simulated EAM of long-term HC variability*

In this section, the spatial pattern of the principal mode of the annual mean HC is analyzed. The explained variance of the first leading mode of the long-term variability of the HC is close to 50% in boreal winter (Ma and Li, 2008), spring (Feng et al., 2013), and summer (Feng et al., 2011), giving us confidence that the first leading mode captures the main variation of the HC. Large differences in the amplitude and structure of the second-and higher-order modes are found in different reanalyses (Feng et al., 2013; Li and Feng, 2015). In addition, in the present study, large discrepancies are apparent in the second and third modes of the annual mean MSF calculated from ERA40 and NCEP/NCAR data, and the second and third modes in the NCEP/NCAR data are not fully separable according to North's rule (not shown). Therefore, only the first leading mode, together with its variability, will be discussed.

The first principal mode of the annual mean HC, in both the NCEP/NCAR and EAR40 data, displays an EAM dominating the variability of the annual mean HC. Note that this

mode is consistently observed in the two reanalysis datasets, and explains ~50% of the variance of the annual mean HC, indicating that this mode can be reliably identified. In fact, this mode is consistently observed in four reanalyses [i.e., NCEP/NCAR, ERA, JRA25 (Japanese 25-year Reanalysis) and the NCEP-DOE (Department of Energy) Reanalysis] within the period 1979–2000 with an explained variance of around 50%, further establishing the robustness of our results. The stronger component of this mode is centered to the north of the equator, extending from 10°S to 30°N. The ascending branch of this component is located to the south of the equator, with a descending branch in the NH. In contrast, the counterpart in the SH is weak in both extent and magnitude, and has its descending branch at ~ 30°S. Note that the first principal mode here is similar to those observed during boreal winter (Ma and Li, 2008) and spring (Feng et al., 2013).

A similar EAM is found in BCC_CSM1_1, BCC_CSM1_1_M, CANESM2, and CNRM_CM5; however, the variances explained by this mode in these models are all much smaller than in observations (Fig. 3). Moreover, the simulated EAM shows large differences in magnitude and extent from that observed. In addition, near-equatorially symmetric structures are observed in the other models, although the mag-

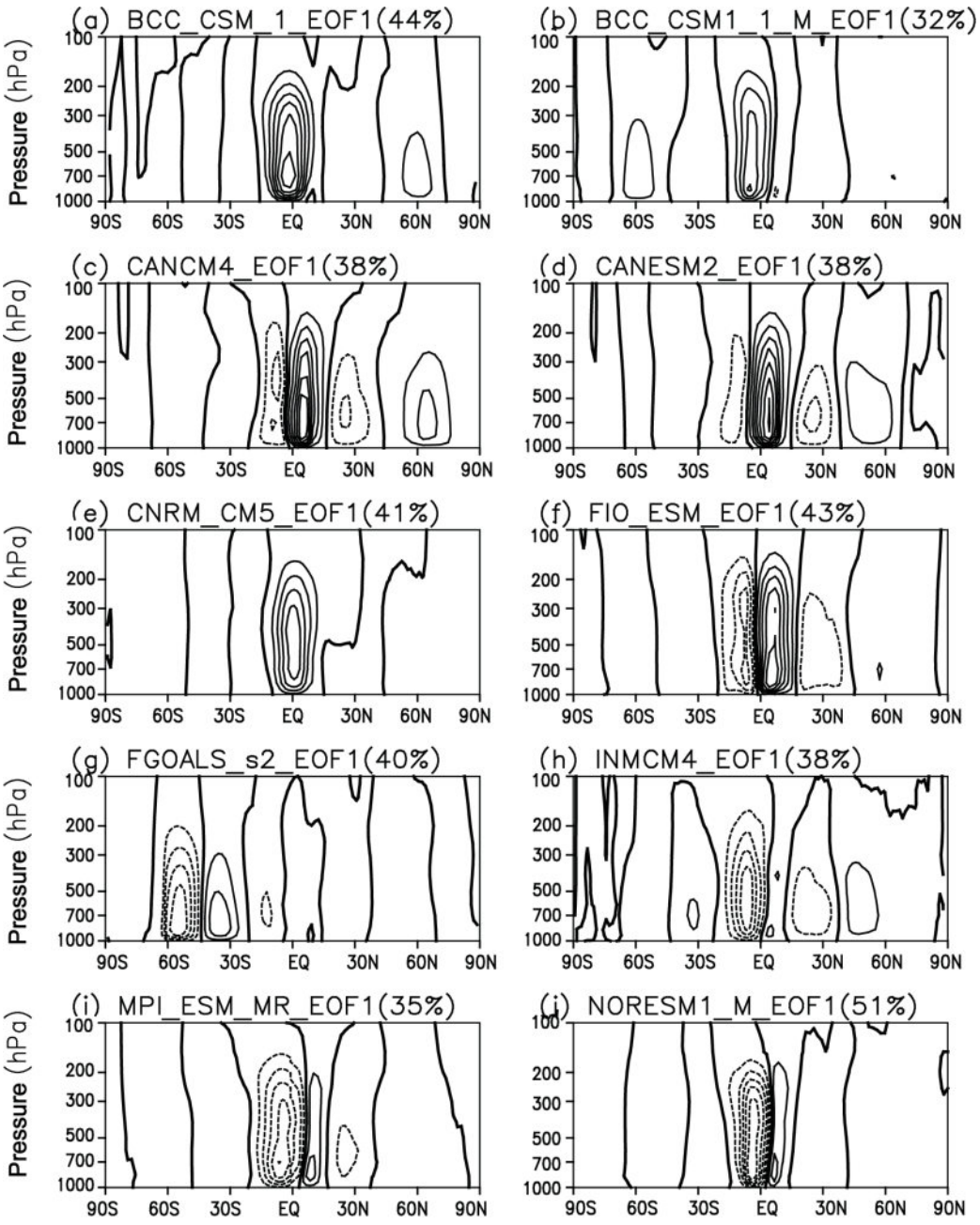

Fig. 3. As in Fig. 1b, but for the first principal mode of the annual mean MSF determined from CMIP5 models over the period 1961–2000.

nitudes of the two components are somewhat different, and the ascending branch is close to the equator, quite different from that observed. To further examine the performance of the models in simulating the variability of the HC, the EOF analysis was repeated exclusively in the low-latitude band (i.e. 45°S–45°N). The result is that the first EOF pattern in the reanalyses is an even stronger EAM with an explained variance of around 95%, indicating the dominance of this mode (not shown). However, the first EOF in the models explains a much smaller variance range from 37.6% (FGOALS-s2) to 60.6% (BCC_CSM_1), and the first EOF modes are not consistent with observations. For example, the first EOF mode is equatorially symmetric in FIO_ESM, and the southern cell dominates—but with an ascending branch around the equator—in MPI_ESM_MR and NORESM1_M (Fig. 4). Note that the first mode in FGOAL-s2 in the low-latitude band analysis is dominated by an equatorially asymmetric cell (Fig. 4g), but when the global domain is examined, it is dominated by extra-tropical circulation, implying an exaggeration of extra-tropical circulation variability in FGOAL-s2 (Fig. 3g). This result suggests that the limited ability of the models to simulate the long-term variability of the HC is not due to poor performance in high latitudes.

The principal components (PCs) of the EAM show similar significant upward trends in both the NCEP/NCAR and ERA40 dataset (Figs. 1e and f), indicating a strengthening of the EAM during 1961–2000, which would intensify the northern component of the HC. The PCs determined from

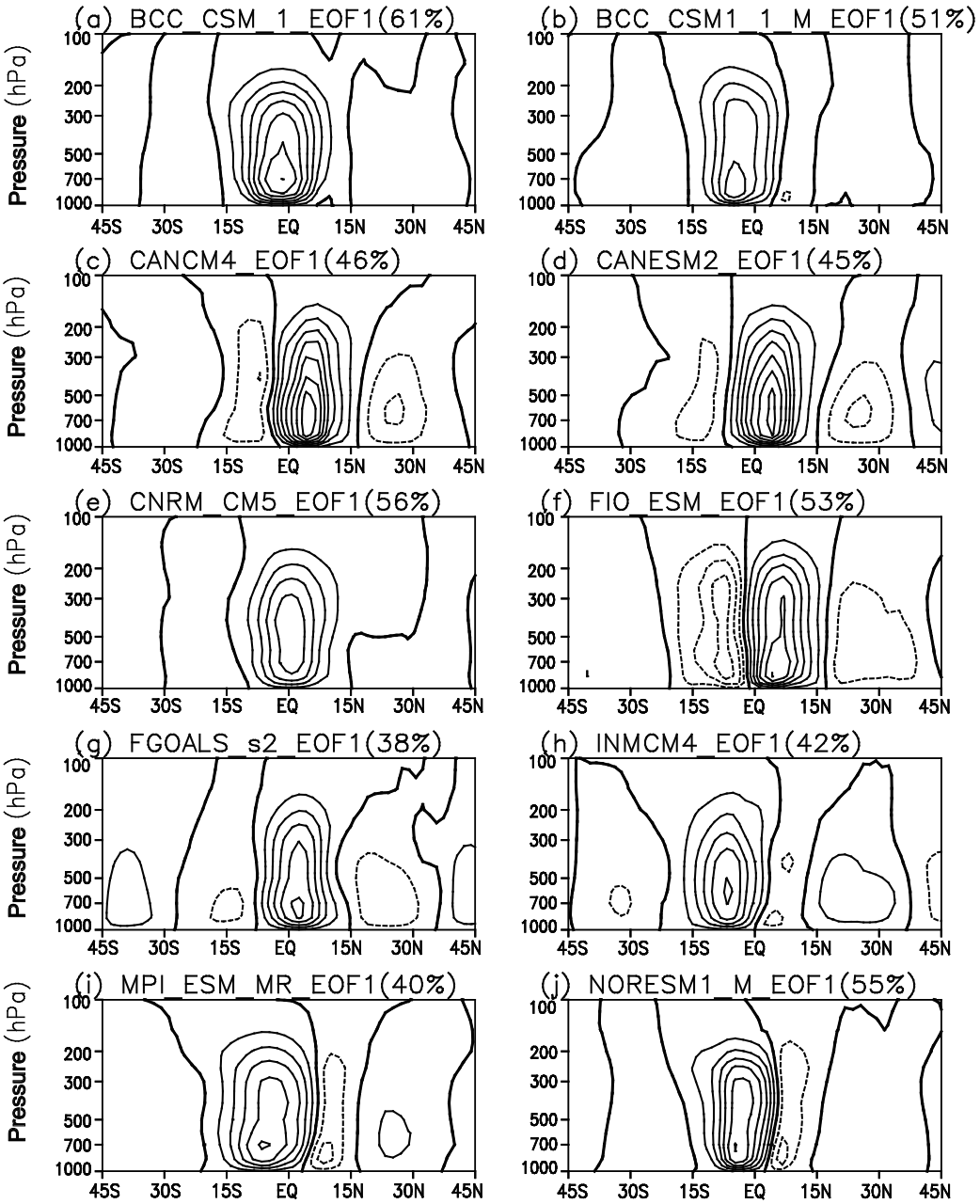

Fig. 4. As in Fig. 3, but for the low-latitude band 45°S–45°N.

the two reanalysis datasets are highly correlated, with a correlation coefficient of 0.91. However, there are many uncertainties in the PCs from the CMIP5 model simulations (Fig. 5). Even those models that successfully simulate the spatial structure of the EAM have PCs with insignificant trends, and none of the correlation coefficients between their interannual variation and that in the reanalyses is significant (see R1 in Table 2). A similar result is seen when the low-latitude band is analyzed, except the significant downward trend in FGOALS-s2 vanishes (not shown). This result implies that none of the models can simulate the long-term trend or the interannual variation of the first leading mode of the annual mean HC variability.

4. Possible causes of the poor simulation of the EAM of the HC

The above results indicate that the CMIP5 models perform poorly in simulating the leading mode of the annual mean HC's long-term variability. In this section, we explore the possible causes of this poor performance for the purpose

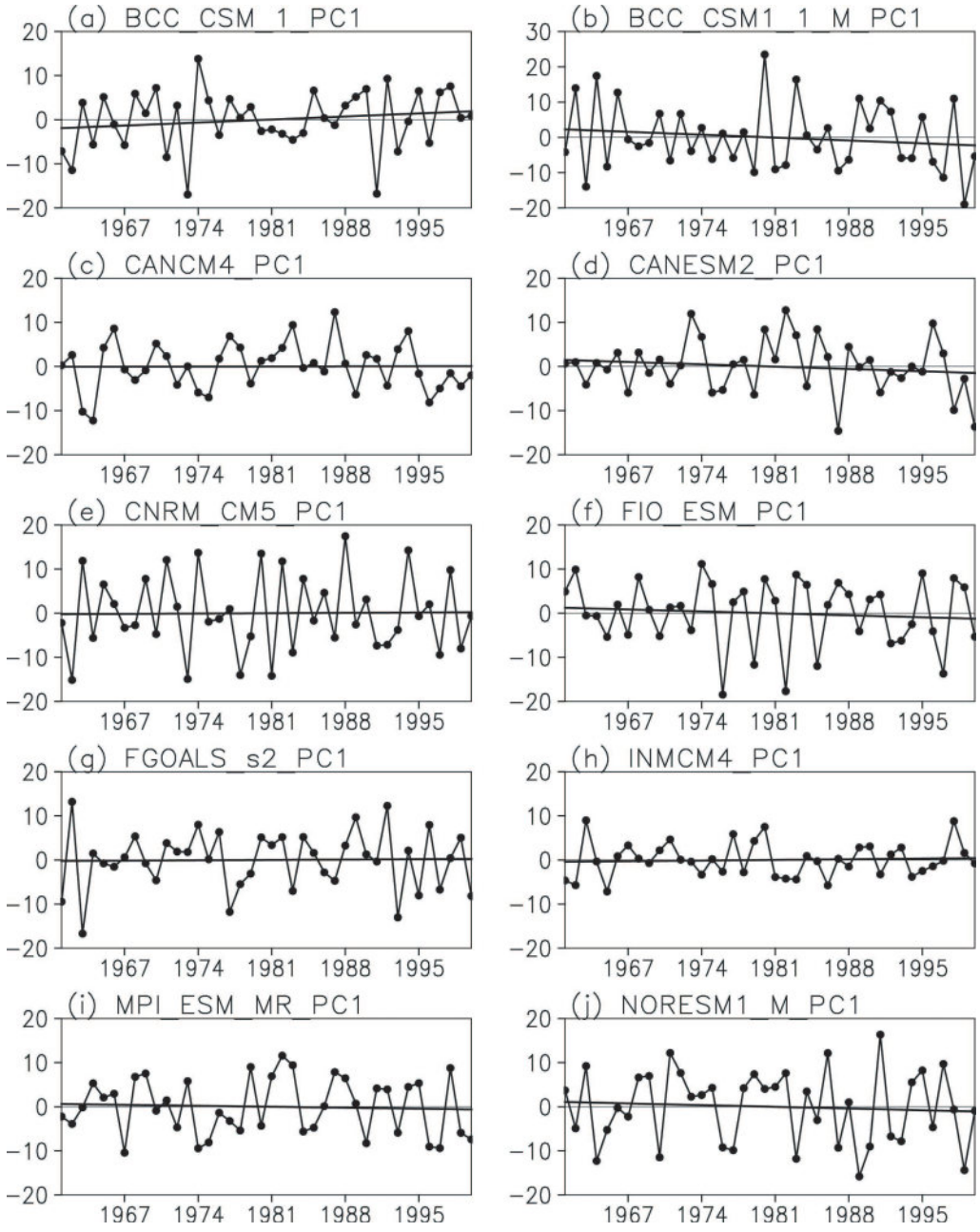

Fig. 5. As in Fig. 1c, but for the time series of the principal mode of the annual mean MSF determined from CMIP5 models over the period 1961–2000. Apart from FGOALS_s2, the linear trends are not significant at the 0.05 level.

of providing some reference points for improving the simulation skill of these models. The HC is a thermally driven meridional circulation, and its variation is closely linked to the underlying thermal structure (Lindzen and Nigam, 1987; Hou and Lindzen, 1992). Therefore, the potential contribution of tropical SST to the variation of the EAM is examined.

First, the distribution of the correlation between the PCs of the EAM and SST is considered, as well as the warming trend of SST during 1961–2000, based on ERSST and HadISST data (Fig. 6). Significant positive correlation over the south of the eastern tropical Pacific, tropical Atlantic, and in the IPWP is apparent (Figs. 6a and b). The areas of significant correlation overlap the regions with a significant warming trend (Figs. 6c and d), indicating that the interannual variation of the PCs is associated with the variation of tropical SST. Note that the warming of tropical SST is equatorially asymmetric (i.e. a stronger signal in the SH than in the NH), and to further explore this, we next consider the temporal evolution of SST averaged over the tropical region in each hemisphere (20°S–0° and 0°–20°N) (Fig. 7). Based on

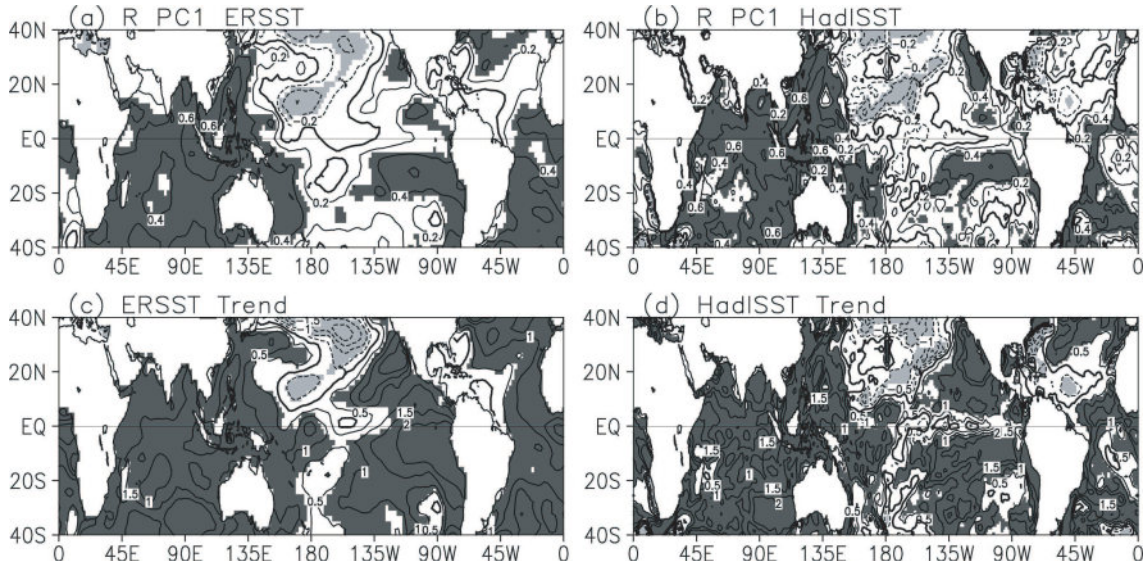

Fig. 6. (a) Spatial distribution of the correlation between the time series of the principal mode for annual mean mass stream function and ERSST. (b) As in (a), but for HadISST. (c) Linear trend of the annual mean ERSST during 1961–2000. (d) As in (c), but for HadISST. Shading indicates statistical significance at the 0.05 significance level (Student's *t*-test).

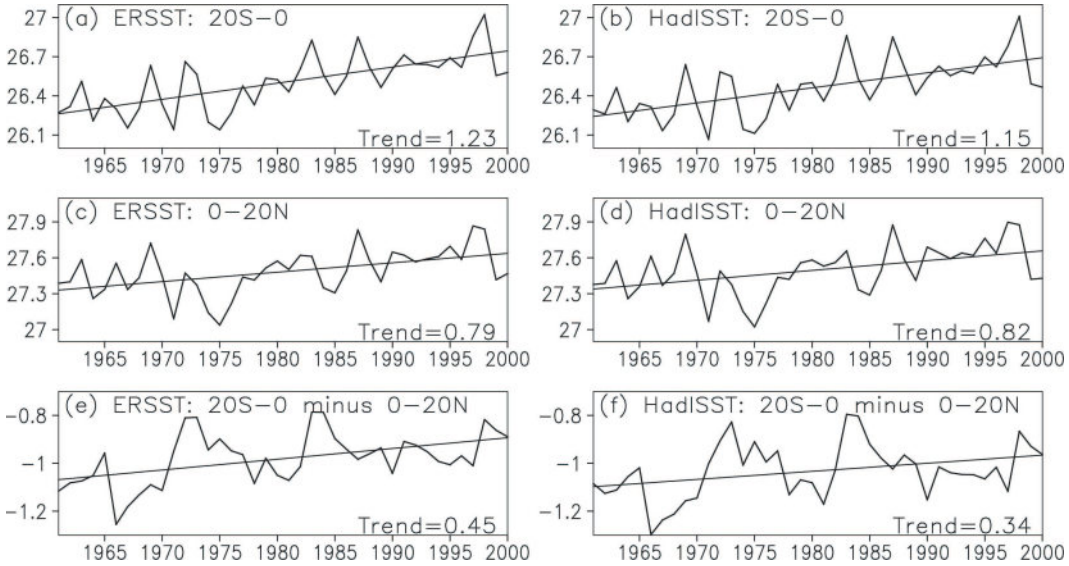

Fig. 7. Time series of SST zonally averaged over (a) 20°S–0° and (b) 0°–20°N, and (c) their difference (black line; unit: °C), as well as their linear trend and the trend coefficients [units: °C (100 yr)$^{-1}$] based on ERSST. (b, d, f) As in (a, c, e), but based on HadISST. The linear trends are all statistically significant at the 0.05 significance level (Student's *t*-test).

ERSST data, both the southern and northern components of averaged SST exhibit significant warming trends, with coefficients of 1.23°C (100 yr)$^{-1}$ and 0.79°C (100 yr)$^{-1}$ respectively from 1961 to 2000. Similarly, based on HadISST, the results are 1.15 and 0.82 °C (100 yr)$^{-1}$. That is, the warming in the tropical SH is more rapid than in the NH in both reanalyses, and this is also clear in their difference (Figs. 7e and f). Their difference [i.e. SST in (20°S–0°) minus SST in (0°–20°N)] shows an obvious upward trend, with a coefficient of 0.45°C (100 yr)$^{-1}$ and 0.34°C (100 yr)$^{-1}$ based on ERSST and HadISST data respectively, both statistically significant at the 0.05 confidence level, indicating that the meridional thermal gradient of the tropics in each hemisphere reduced during 1961–2000. As shown theoretically by Feng et al. (2013), the anomalous spatial pattern of HC is closely linked to the structure of the meridional thermal gradient. Furthermore, they also established that the location of the ascending branch of the anomalous HC corresponds exactly to the position where the SST meridional gradient passes through zero from positive to negative. The possible influence on the HC of the SST difference between the southern and northern tropics can be further seen from the composite difference in the HC MSF between the years of larger and smaller SST difference (Fig. 8). The variation of the tropical hemisphere gradient is associated with an anomalous vertical circulation with anomalous ascent located in the SH, similar to the EAM of the HC. This implies that the difference between the tropical SH and NH SST contributes to the intensity of the EAM.

Accordingly, we further explore the long-term trends of SST in the CMIP5 model results (Fig. 9). The significant warming trends in the IPWP and tropical Atlantic are captured well by all the models, but not the warming in the south of the eastern tropical Pacific. In addition, the cooling in the north of the central Pacific is not reproduced in all the models. The quality of the simulation of the long-term trend of SST within the tropics (i.e. 20°S–20°N, 0°–360°E) is further seen in the spatial correlation coefficients between the observations (based on ERSST; R2 in Table 2) and the models. The correlation coefficients are all above 0.34, indicating a reasonable response of the model simulations to the underlying thermal forcing.

Next, we consider the temporal evolution of the tropical SST in each hemisphere, as well as the SST meridional gradient (Fig. 10). The simulated warming trends within the tropics in each hemisphere in BCC_CSM1_1, CANESM2, FGOALs_s2, and MPI_ESM_MR are larger than observed, while they are much smaller in INMCM4. Notwithstanding the consistent warming trends, most of the models cannot reproduce the long-term trends in the SST meridional gradient (Fig. 11). Only two models (BCC_CSM1_1 and CANCM4) show the long-term upward trends in the warming differences between the SH and NH seen in the reanalyses, but these trends are not significant in these models. Also, the correlation of the meridional SST gradients in BCC_CSM1_1 and CANCM4 with those in ERSST is 0.04 and 0.16 respectively, and neither is statistically significant, even at the 0.2 level. This suggests that the ability of the models to reproduce the meridional gradient of tropical SST within the two hemispheres is unacceptable, for either spatial or interannual variation, and leads to incorrect simulation of the long-term variability of the EAM. Moreover, the observed SST difference between the southern and the northern tropics is around 1° with ±0.1° variation in time. However, it ranges from around 0.1° to around 0.7° in the CMIP5 models, implying a smaller meridional SST gradient between the SH and NH in the CMIP models than in the reanalyses. This may be the reason why the explained variance of the first EOF in the models is much smaller than in the reanalyses. Note that although the only difference between BCC_CSM1_1 and BCC_CSM1_1_M is the resolution, their simulations of the HC differ considerably, suggesting that resolution has a major impact on the model simulations.

The discussion above indicates that most of the simulations of the underlying thermal forcing in CMIP5 models are inconsistent with observations, which may explain the poor simulation of the spatial structure and temporal evolution of the EAM.

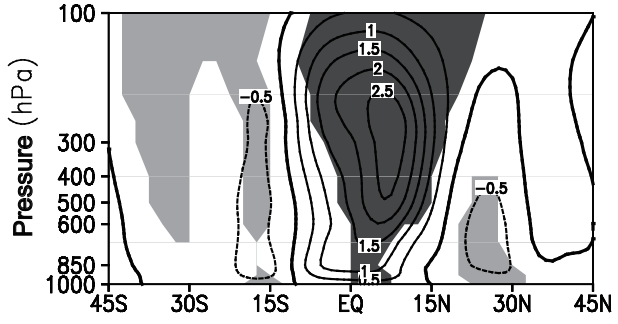

Fig. 8. Composite differences of mass stream function between years with larger and smaller differences between the tropical Southern Hemisphere and Northern Hemisphere. Shading indicates statistical significance at the 0.05 significance level (Student's *t*-test).

5. Discussions and Conclusion

This study investigated the simulation of the climatological characteristics of the annual mean HC, its spatial structure, and the temporal evolution of the long-term variability of the principal mode of the annual mean HC, using 10 CMIP5 models. The results showed that the selected models can capture the spatial structure of the climatological HC reasonably well, including its extent and strength. However, this is not the case for the long-term variability of the principal mode of the annual mean HC, the EAM, either in terms of its spatial pattern or interannual variation. It was found that only four models (BCC_CSM1_1, BCC_CSM1_1_M, CANESM2, and CNRM_CM5) can reproduce the equatorially asymmetric structure of the principal mode, consistent with reanalysis data, but with smaller explained variance, implying limited skill in depicting the spatial pattern of the EAM. Fur-

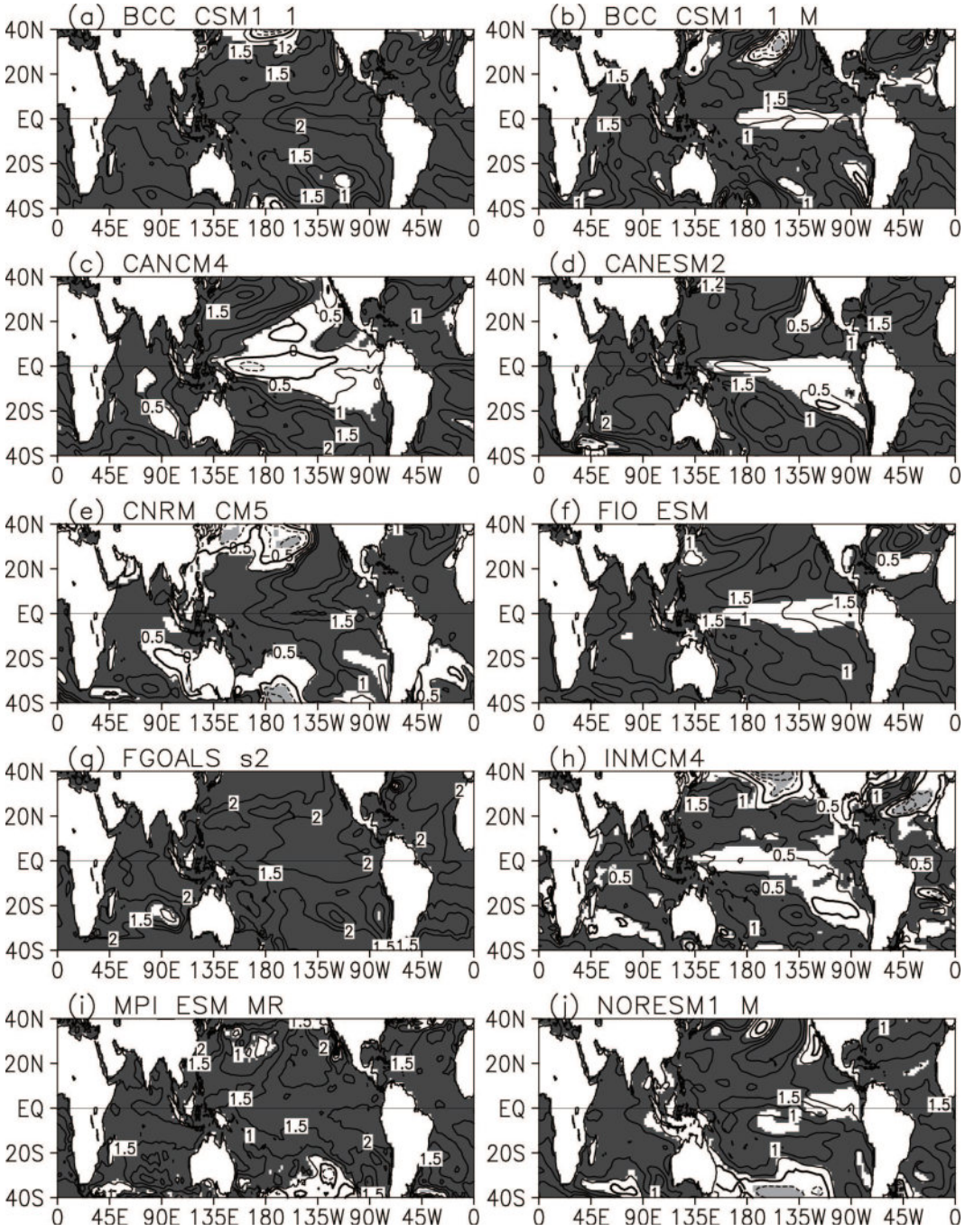

Fig. 9. As in Fig. 6b, but based on CMIP5 models.

thermore, none of the models can satisfactorily reproduce the interannual variation of the EAM or the long-term trend, indicating poor skill in reproducing the variability of the annual mean HC. This poor performance in simulating the long-term variability of the EAM meant that we did not attempt to investigate the possible variation of the HC in the future under different climate change scenarios.

The possible reasons for the poor performance of the CMIP5 models in simulating the long-term variability of the EAM were examined. Since the HC is mainly a thermally driven circulation, and as the warming within the tropics has been reported to have key impacts on the long-term variability of the HC (Feng et al., 2013; Li and Feng, 2015), we discussed the potential influence of such warming on the HC in the CMIP5 models. All the models considered exhibit encouraging warming trends within the tropical oceans; however, most display a reversed warming speed between the tropical SH and NH compared with observations. In observations, the warming within the tropical SH is faster than that in the NH, and the meridional gradient of the tropical SH and NH has reduced in recent decades. However, only two of the models (BCC_CSM1_1 and CANCM4) show similar

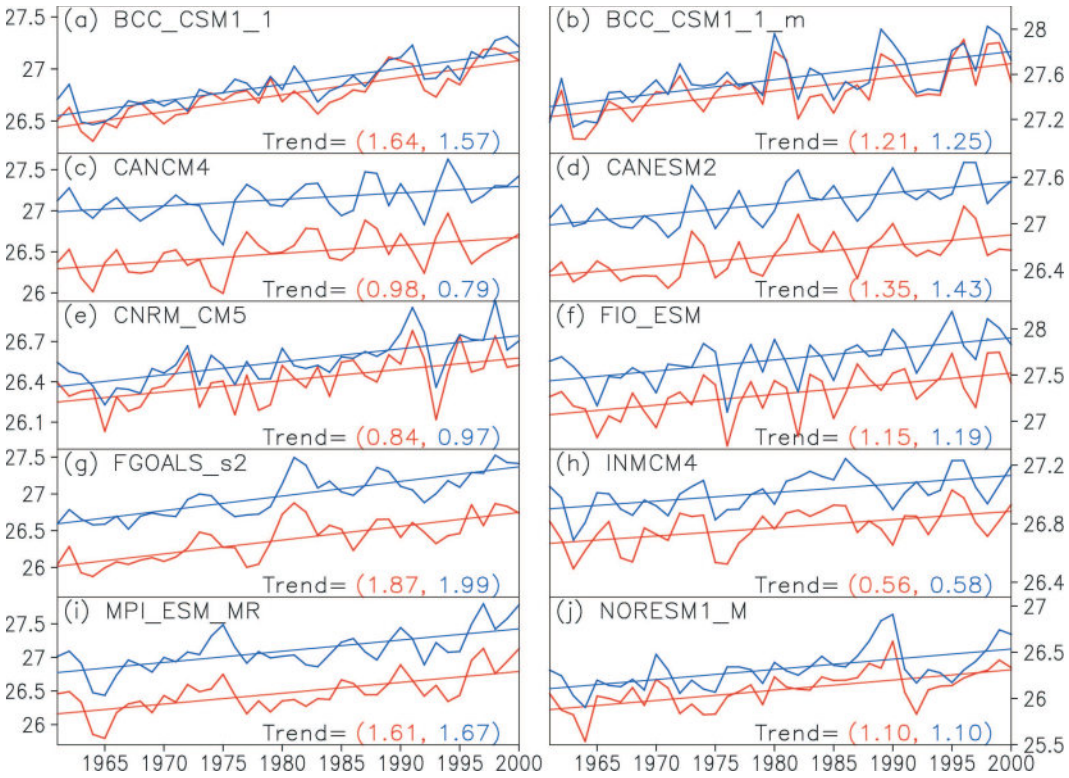

Fig. 10. As in Fig. 7, but based on CMIP5 models. Red and blue lines are for the SST spatially averaged within 20°S–0° and 0°–20°N, respectively. All of the trends are statistically significant at the 0.05 significance level (Student's *t*-test).

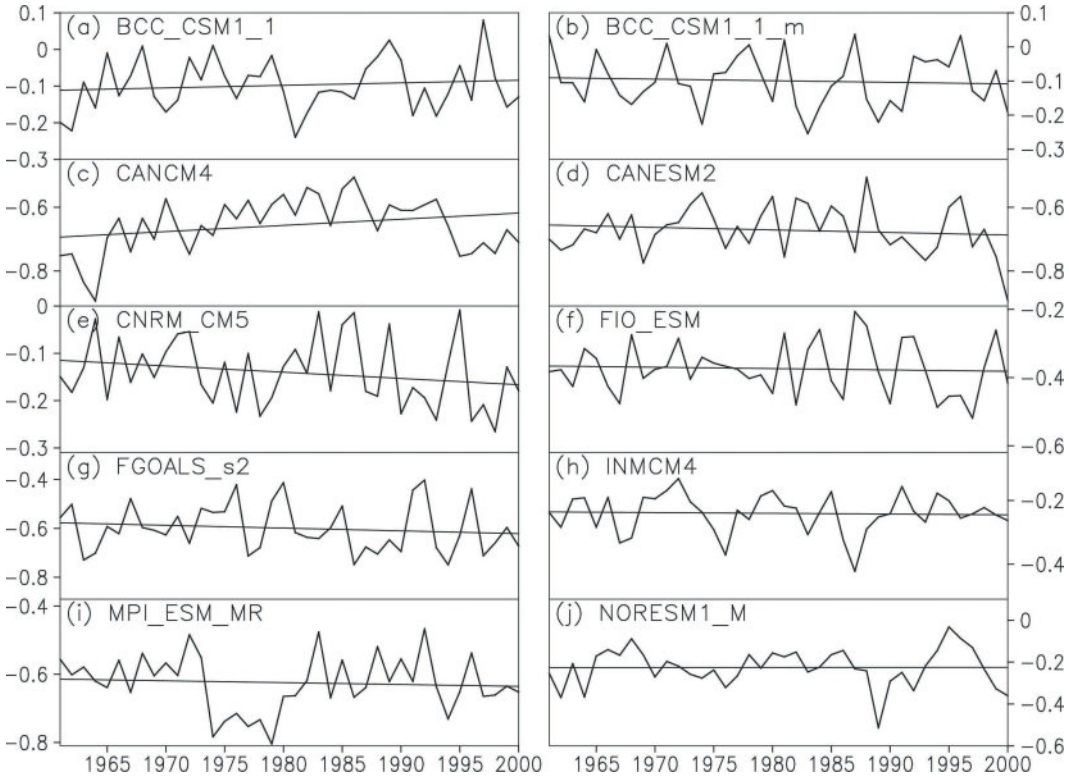

Fig. 11. As in Fig. 7c, but based on CMIP5 models.

differences in warming, and these changes in meridional gradient are poorly correlated with observations. This demonstrates that the limited skill in simulating the underlying thermal variation within the tropics may contribute to the poor ability of the models to reproduce the long-term variability of the EAM. On the other hand, the magnitude of the gradient within the tropical hemispheres is much smaller than observed, which may also contribute to the poor simulation of the EAM.

This study did not identify why the models cannot reproduce the warming differences between the tropical SH and NH, since the variation of the underlying SST is a complex issue that is not only linked to atmospheric processes, but is also affected by processes in the interior ocean, as well as air–sea interaction. Nevertheless, a possible cause of the poor simulation by CMIP5 models of the long-term variability of the principal mode of the annual mean HC is highlighted in this paper, and we hope the result will be helpful in improving CMIP5 model simulations.

Acknowledgements. This work was jointly supported by the National Natural Science Foundation of China (Grant Nos. 41205046 and 41475076), the 973 Program (Grant No. 2013CB 430203). We thank the World Climate Research Programme's Working Group on Coupled Modeling, which is responsible for CMIP, and the climate modeling groups (listed in Table 1 of this paper) for producing and making available their model output.

REFERENCES

Bao, Q., and Coauthors, 2013: The flexible global ocean-atmosphere-land system model, version 2: FGOALS-s2. *Adv. Atmos. Sci.*, **30**, 561–576, doi: 10.1007/s00376-012-2113-9.

Bentsen, M., and Coauthors, 2012: The Norwegian earth system model, NorESM1-M—part 1: Description and basic evaluation. *Geosci. Model Dev. Discuss.*, **5**, 2843–2931.

Chylek, P. J., J. Li, M. K. Dubey, M. Wang, and G. Lesins, 2011: Observed and model simulated 20th century Arctic temperature variability: Canadian Earth system model CanESM2. *Atmos. Chem. Phys. Diss.*, **11**, 22 893–22 907.

Chang, E. K. M., 1995: The influence of Hadley circulation intensity changes on extratropical climate in an idealized model. *J. Atmos. Sci.*, **52**, 2006–2024.

Chen, J. Y., B. E. Carlson, and A. D. Del Genio, 2002: Evidence for strengthening of the tropical general circulation in the 1990s. *Science*, **295**, 838–841.

Diaz, H. F., and R. Bradley, 2004: *The Hadley Circulation: Present, Past and Future*. Kluwer Academic Publishers, The Netherlands, 511 pp.

Dima, I. M., and J. M. Wallace, 2003: On the seasonality of the Hadley cell. *J. Atmos. Sci.*, **60**, 1522–1527.

Feng, J., and J. P. Li, 2013: Contrasting impacts of two types of ENSO on the boreal spring Hadley circulation. *J. Climate*, **26**, 4773–4789.

Feng, R., J. P. Li, and J. C. Wang, 2011: Regime change of the boreal summer Hadley circulation and its connection with the tropical SST. *J. Climate*, **24**, 3867–3877.

Feng, J., J. P. Li, and F. Xie, 2013: Long-term variation of the principal mode of boreal spring Hadley circulation linked to SST over the Indo-Pacific warm pool. *J. Climate*, **26**, 532–544.

Fu, Q., C. M. Johanson, J. M. Wallace, and T. Reichler, 2006: Enhanced mid-latitude tropospheric warming in satellite measurements. *Science*, **312**, 1179.

Frierson, D. M. W., J. Lu, and G. Chen, 2007: Width of the Hadley cell in simple and comprehensive general circulation models. *Geophys. Res. Lett.*, **34**(18), L18804, doi: 10.1029/2007GL 031115.

Guo, Y., W. J. Dong, F. M. Ren, Z. C. Zhao, and J. B. Huang, 2013: Assessment of CMIP5 simulations for China annual average surface temperature and its comparison with CMIP3 simulations. *Progressus Inquisitiones De Mutatione Climatis*, **9**(3), 181–186. (in Chinese)

Hou, A. Y., 1998: Hadley circulation as a modulator of the extratropical climate. *J. Atmos. Sci.*, **55**, 2437–2457.

Hou, A. Y., and R. S. Lindzen, 1992: The influence of concentrated heating on the Hadley circulation. *J. Atmos. Sci.*, **49**(14), 1233–1241.

Hu, Y. Y., and C. Zhou, 2009: Decadal changes in the Hadley circulation. *Adv. Geosci.*, J. H. Oh, Ed., World Scientific Publishing Company, Singapore, 250 pp.

Hu, Y. Y., C. Zhou, and J. P. Liu, 2011: Observational evidence for poleward expansion of the Hadley circulation. *Adv. Atmos. Sci.*, **28**(1), 33–44.

Hu, Y. Y., L. J. Tao, and J. P. Liu, 2013: Poleward expansion of the Hadley circulation in $CMIP_5$ simulations. *Adv. Atmos. Sci.*, **30**(3), 790–795.

Hudson, R. D., M. F. Andrade, M. B. Follette, and A. D. Frolov, 2006: The total ozone field separated into meteorological regimes-part II: Northern Hemisphere mid-latitude total ozone trends. *Atmos. Chem. Phys.*, **6**, 5183–5191.

Johanson, C. M., and Q. Fu, 2009: Hadley cell widening: Model simulations versus observations. *J. Climate*, **22**, 2713–2725.

Kalnay, E., and Coauthors, 1996: The NCEP/NCAR 40-year reanalysis project. *Bull. Amer. Meteor. Soc.*, **77**, 437–472.

Li, J. P., 2001: *Atlas of Climate of Global Atmospheric Circulation I. Climatological Mean State*. China Meteorological Press, Beijing, 279 pp. (in Chinese)

Li, J. P., and J. Feng, 2015: Tropical large-scale atmosphere-ocean interaction in association with subtropical aridity trend. *On Aridity Trend in Northern China*. C. B. Fu., Ed., World Scientific. (in press)

Lindzen, R. S., 1994: Climate dynamics and global change. *Annual Review of Fluid Mechanics*, **26**, 353–378.

Lindzen, R. S., and S. Nigam, 1987: On the role of sea surface temperature gradients in forcing low-level winds and convergence in the tropics. *J. Atmos. Sci.*, **44**, 2418–2436.

Lu, J., G. A. Vecchi, and T. Reichler, 2007: Expansion of the Hadley cell under global warming. *Geophys. Res. Lett.*, **34**, L06805, doi: 10.1029/2006GL028443.

Jiang, Y., Y. Luo, and Z. C. Zhao, 2010: Projection of wind speed changes in China in the 21st century by climate models. *Chinese J. Atmos. Sci.*, **34**, 323–336.

Ma, J., and J. P. Li, 2008: The principal modes of variability of the boreal winter Hadley cell. *Geophys. Res. Lett.*, **35**, L01808, doi: 10.1029/2007GL031883.

Nguyen, H., A. Evans, C. Lucas, I. Smith, and B. Timbal, 2013: The Hadley circulation in reanalyses: Climatology, variability, and change. *J. Climate*, **26**, 3357–3376.

Qiao, F. L., Z. Y. Song, Y. Bao, Y. J. Song, S. Qi, C. J. Huang, and W. Zhao, 2013: Development and evaluation of an earth system model with surface gravity waves. *J. Geophys. Res.*,

118, 4514–4524.

Quan, X. W., H. F. Diaz, and M. P. Hoerling, 2004: Change in the tropical Hadley cell since 1950. *The Hadley Circulation: Present, Past and Future*, H. F. Diaz and R. S. Bradley, Eds., Springer, 85–120.

Rayner, N. A., D. E. Parker, E. B. Horton, C. K. Folland, L. V. Alexander, D. P. Rowell, E. C. Kent, and A. Kaplanand, 2003: Global analyses of sea surface temperature, sea ice, and night marine air temperature since the late nineteenth century. *J. Geophys. Res.*, **104**(D14), 4407, doi: 10.1029/2002JD002670.

Seidel, D. J., Q. Fu, W. J. Randel, and T. J. Reichler, 2008: Widening of the tropical belt in a changing climate. *Nature Geoscience*, **1**, 21–24.

Smith, T. M., and R. W. Reynolds, 2004: Improved extended reconstruction of SST (1854–1997). *J. Climate*, **17**, 2466–2477.

Stachnik, J. P., and C. Schumacher, 2011: A comparison of the Hadley circulation in modern reanalyses. *J. Geophys. Res.*, **116**, D22102, doi: 10.1029/2011JD016677.

Stevens, B., and Coauthors, 2013: The atmospheric component of the MPI-M Earth system model: ECHAM6. *J. Adv. Model Earth Syst.*, **5**, 146–172.

Taylor, K. E., R. J. Stouffer, and G. A. Meehl, 2012: An overview of CMIP5 and the experiment design. *Bull. Amer. Meteor. Soc.*, **93**, 485–498.

Uppala, S. M., and Coauthors, 2005: The ERA-40 re-analysis. *Quart. J. Roy. Meteor. Soc.*, **131**, 2961–3012.

Voldoire, A., and Coauthors, 2013: The CNRM-CM5.1 global climate model: Description and basic evaluation. *Climate Dyn.*, **40**, 2091–2121.

Volodin, E. M., N. A. Dianskii, A. V. Gusev, 2010: Simulating present-day climate with the INMCM4.0 coupled model of the atmospheric and oceanic general circulations. *Atmos. Ocean. Phy.*, **46**(4), 414–431.

Wielicki, B. A., and Coauthors, 2002: Evidence for large decadal variability in the tropical mean radiative energy budget. *Science*, **295**, 841–844.

Zheng, F., J. P. Li, R. T. Clark, and H. C. Nnamchi, 2013: Simulation and projection of the Southern Hemisphere Annular Mode in CMIP5 models. *J. Climate*, **26**, 9860–9879.

Zhu, X., W. J. Dong, and Y. Guo, 2013: Comparison of simulated winter and spring Arctic oscillation variability by CMIP5 and CMIP3 coupled models. *Progressus Inquisitiones De Mutatione Climatis*, **9**(3), 165–172. (in Chinese)